An Electric Vehicle with Novel Powertrain

Gerry Chen, Zhongxi Li, Stefan M. Goetz, Angel V. Peterchev

April 15, 2019

Abstract

The modular multilever series parallel converter (MMSPC) is a new power supply topology which has a broad set of applications in power electronics including medical, audio, transmission, and motor fields. This research focuses on the use of an MMSPC system for brushless DC (BLDC) motor control. The chief advantages of modular multilever converter (MMC) systems in BLDC motor control hinge on their abilities to generate better granularity in voltage by dynamically reconnecting battery power supplies to generate true analog voltages at very high powers. The MMSPC topology extends upon this advantage by providing auto-balancing capabilities. In this paper, the design and implementation of the MMSPC-motor system is described as well as algorithms for the control of the motor including rotor angle estimation from hall sensor inputs and field oriented control.

Contents

1 Introduction

The MMC is a class of topologies which consists of multiple battery modules, of which a subset can be selected to connect in series to generate a higher system voltage. One such implementation (half bridge topology) is shown in Figure 1a for clarity. MMCs have become common in high power and high voltage applications due to their numerous advantages. By splitting the system voltage into a sum of smaller voltages, an MMC can generate a finite set of true analog voltages and can produce intermediate voltages via pulse width modulation (PWM) with less switching losses than traditional PWM systems. This enables higher fidelity signals in high power applications, reduced switching losses, and lower cost components due to lower voltage limits. An additional advantage of MMC systems is their modularity. Since modules can be made identical, manufacturing and assembly can be simplified and the same modules can be reconfigured for a wide variety of applications.

The MMSPC is a relatively novel topology which allows for connecting module cells not only in series, but also in parallel [3]. The circuit topology is shown in Figure 1b. The primary advantage of this topology is the ability to passively balance the battery cells by periodically applying parallel mode thereby eliminating the need for high-speed balancing sensors and high speed balancing control. An apparent downside of the topology is the increased semiconductor demand, but since the current through each module is always split between two H-bridges, in fact actually the semiconductor area required is the same as for a comparable MMC module capable of producing negative voltages (full bridge topology). In this respect, the MMSPC has significant advantages where longevity, flexibility, and robust control of a modular power solution are required.

(a) Example MMC implementation with 3 half-bridge modules

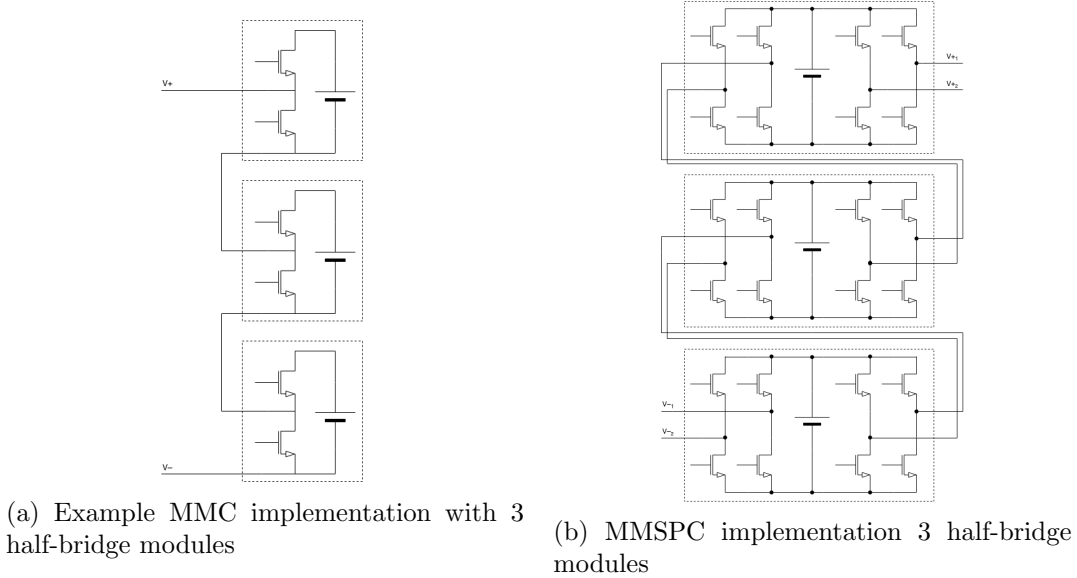(b) MMSPC implementation 3 half-bridge modules

Figure 1: MMC topology comparison

One such application where MMSPCs bring significant advantages is brushless DC (BLDC) motor control. BLDC motor control requires three highly dynamic analog voltages to drive the motor efficiently. Traditional BLDC motor control involves applying PWM

across the full system bus volage to three H-bridges: one for each motor winding phase. The PWM causes significant stress on both the semiconductors and the motor thereby increasing system cost and reducing motor torque. It also results in significant switching losses. MMC systems significantly mitigate these issues but require complex control schemes to maintain battery cell balancing. However, robust balancing is imperative in the industrial and automotive applications in which BLDC motors are often used. Therefore, MMSPCs offer significant advantages for this application. The long term goal of the project is to implement the system in an automobile to test and compare the system to a traditional, non-modular motor control and battery management system. In this paper, an MMSPC system for controlling a 2.2kW BLDC motor and the accompanying challenges are described.

First, an overview of the system architecture is described. Then, some pertinent details and analysis regarding the system construction are discussed. Finally, details of the motor control are discussed. To take full advantage of the MMSPC, field oriented control (FOC) is used for motor control, but one of the primary challenges with implementing FOC is obtaining accurate rotor position information using reliable, low cost sensors. Thus, first an analysis is performed for various rotor angle estimation techniques. Then, an analysis of MMSPC on system performance as compared to a standard DC bus is performed. Conclusions as to the theoretical and practical viability of MMSPC in motor control applications are made.

2   System Overview

The MMSPC motor controller system consists of:

- 12 MMSPC modules

- sbRIO-9627 board and custom "motherboard"

- BM1424ZXF-2.2KW72V motor

The overall assembly is shown in Figure 2 and each subpart is described below. Note that the setup as shown in Figure 2 is configured for bench-testing purposes. In the final system, the control board will be mounted underneath the modules and the modules will be covered by a protective acrylic box. The batteries will also be placed inside the black aluminum module boxes. Thus, the only interface between the MMSPC system enclosure and outside world will be for the 3 phase wires, hall sensors, and ethernet computer interface for data collection.

2.1   MMSPC modules

The MMSPC modules are connected in three sets of four modules. Each phase set of four modules is used to control one motor phase thereby allowing true analog increments of 25% of the maximum system voltage.

Each MMSPC module uses a custom switching board which includes isolated gate drivers for controlling the switching MOSFETs. A photo is shown in Figure 3. Each module used a 1.2Ah 12V SLA battery during testing for safety reasons, but the final implementation
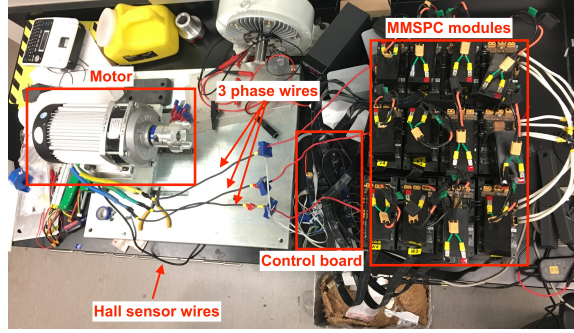
Figure 2: MMSPC motor control system

on the test vehicle will use three, 5200mAh 3s LiPo batteries per module. The batteries are intended to be housed inside the black metal cases.

The modules each have three battery connectors, a pair each of input/output connector (four in total), and logic input signals. The output of each module is the input of the next module in the phase set. The inputs to the first modules in each phase set are connected together to form the virtual ground point. The outputs of the last modules in each phase set go to the motor phases. The choice of which of the two outputs to use for the phase wires on the last module is irrelevant since the redundant output is only used for parallelizing/balancing purposes. The logic input signals consist of logic ground/power and a high side and low side signal for each of the four h-bridges (8 switching signals in total).
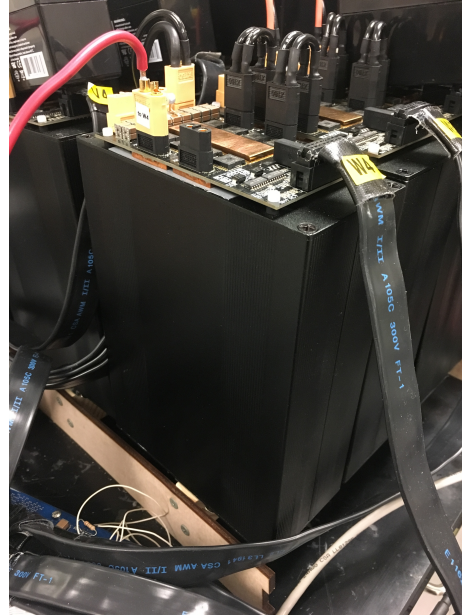

Figure 3: MMSPC module with battery, interconnects, and logic inputs

2.2 Control Boards

The sbRIO-9627 board is shown in Figure 4 and is part of the NI RIO ecosystem. Programming for the system is done in Labview and compiled with Xilinx tools. The board features a 667MHz CPU, Zynq-7020 Xilinx FPGA, and peripheral support. Of the 100 digital I/Os, 96 are required for switching the 12 MMSPC modules and 3 are required for interpreting the hall sensors. Of the 16 analog inputs, 3 are required for reading the phase currents which are transduced with LA 150-P current sensors and amplified with current sense amplifiers. Analog outputs are used for debugging and data collection purposes.

Figure 4: sbRIO-9627 module with 3 current sense inputs, 3 hall sensor inputs, and 96 MMSPC logic outputs

3 Module Construction

From a mechanical design perspective, several aspects of the MMSPC modules required consideration to ensure safe operation in an automotive environment:

- Thermal design for heat dissipation in batteries and semiconductors

- Structural mounting of batteries and electrical boards

- Structural mounting of twelve modules in secure assembly

After running the system under typical operating conditions and subjecting the powered-off setup to vibration, no damage was found preliminarily confirming the structural and thermal integrity of the system.

3.1 Thermal Considerations

Although approximate thermal calculations for MOSFET heat sinking were performed during board design, additional analysis was required due to uncertainty in switching losses, extraneous losses, and conduction/convection coefficients. Two tests were done to analyze the effect of switching frequency and conduction losses for two choices of MOSFETs and for three different switching frequencies. The boards were run under the desired load conditions and the temperature was measured over a duration of one minute to make comparative measurements. The results for the switching and conduction loss tests are shown in Figures 5a and 5b respectively. The tests show that conduction losses are of far greater concern, logging nearly 15°C of temperature difference over a minute in the worst case of 80A. Thus, the choice was made to use the "version 04" MOSFETs which feature lower $R_{DS,on}$ at the expense of higher gate capacitances.

When considering the overall thermal design, it is important to note that the aforementioned tests were conducted without any heat sinking or active air flow. The boards were tested as-designed. The 80A test appears to indicate that the temperature has begun to stabilize and has reached approximately 70% of its final value according to an exponential decay regression as per the lumped capacitance model of transient temperature change. Accordingly, the temperature of the MOSFET cases at 80A is expected to stay within 11°C of ambient and thus poses no concern for overheating.
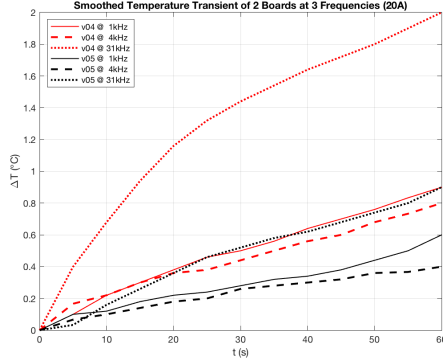
(a) Switching losses comparison for two different MOSFET choices at three different switching frequencies
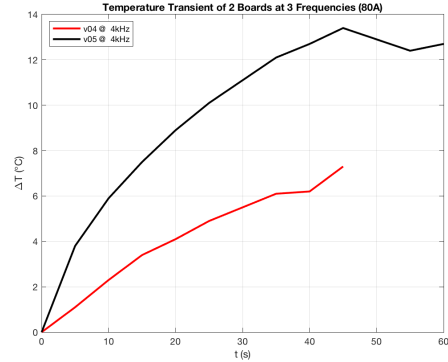
(b) Comparison of two different MOSFET choices at high current

Figure 5: Thermal analysis of MMSPC boards

3.2 Single Module Assembly

The core of the MMSPC modules is a metal box large enough to house three 5200mAh, 3s LiPo batteries and wide enough to accomodate the electrical boards on the lid.

The batteries are to be potted into the box with their connectors reaching through a rectangular hole CNC milled into the lid of the box. For testing purposes, alternate batteries were used and placed outside of the box for easy assembly and disassembly.

As shown in Figure 6, the MMSPC boards are affixed to the metal casing of the module boxes with four bolts/standoffs and an electrically insulating sil-pad with a thermal resistance of $0.024°C/W$ bridging the thermal path from the bottom side MOSFETs to the metal box. Again, the heat dissipation will clearly not be a concern.
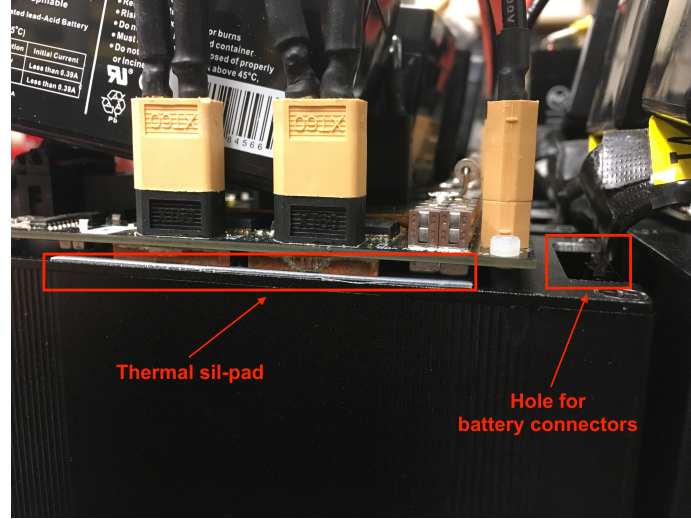

Figure 6: MMSPC module electrical mounting and rectangular hole for battery connectors

3.3 Overall Modules assembly

The module boxes are arranged in three sets of four rows with a 10mm gap between rows to allow the signal wires to reach the control board underneath the modules. The are mounted on DIN-rail mounts with two mounting prongs per module and one rail per phase set of four modules. The DIN-rail is rigidly mounted and fixed to a wooden base structure. The modules are covered by an acrylic protective box to protect from environmental factors.

A planned upgrade is to replace the wooden base with aluminum square tubes for better structural support. An additional aluminum flat rod is intended to be installed perpendicular to the DIN-rail to reinforce it as well.

Although the control board was not set up in its final intended position for testing, it is planned to be placed underneath the modules so that there is easy access for the logic wires. In this position, only the phase wires, hall sensors, and data collection ethernet cable need to be connected outside of the protective housing. To get a preliminary test of robustness, the system was placed (powered off) in the trunk of a Honda CRV and driven for over 50 miles. No damage was found.

4 Rotor Angle Estimation

4.1 Introduction

FOC and other motor control schemes necessarily require precise rotor angle information. Although there exists some literature for estimating rotor position using both sensorless

Figure 7: 12 MMSPC modules in their protective case

methods [1] and encoders/resolvers, both have limitations. Estimation by sensorless methods has the severe limitation of relying on software which, when a reliable estimate cannot be made, results in total system failure and the possibility of being impossible to safely shutdown in the case of field-weakening. Rotor position determination through the use of encoders is typically expensive and may also be prone to hardware malfunction if not installed properly or of low quality. Therefore, resolvers are most commonly used in automotive and critical industrial applications, but they are typically very costly.

Angle estimation through the use of hall sensors provides several key features, however, that make it a viable option for automotive and industrial motor control applications given sufficient research. First, hall sensors are very reliable and very rarely fail. Second, not only is the hardware reliable, but the trapezoidal control using hall sensors is also sufficiently simple that, in the event of total system failure, a discrete hardware circuit can be used as a fallback to maintain safe operation. Finally, hall sensors are extremely commonplace and inexpensive. In this direction, the existing motor for our MMSPC setup has been adapted from a go-cart/dune-buggy kit and has pre-existing hall sensors on account of being originally driven by the stock controller with trapezoidal control. Therefore, the detour to investigate hall sensor based rotor angle estimation is very natural.

4.2 Overview of Techniques

The two primary techniques analyzed are a first-order extrapolation and a single-PI phase locked loop (PLL).

In the first-order extrapolation, the velocity is estimated using the previous two hall sensor transitions and the position is extrapolated until the next hall sensor transition. Importantly, during the extrapolation, a constraint is applied to ensure that the extrapolated position never exceeds one hall sensor transition away from the current hall sensor reading. This estimation scheme is similar to [2] in the way the position estimation is bounded by the hall sensor transitions and similar to the scheme proposed in [4] in the estimation method, described there as the "zero-order Taylor Algorithm". As pointed out by [5], however, this method is plagued by issues arising from hall sensor misalignment and missed transitions. Both of these issues cause significant estimation errors, discontinuous estimations and derivatives, and noisy velocities. Despite these issues, this method is still a

reasonably suitable first-pass approach and yields reasonable results. The issue is mitigated to a degree by calibrating for hall sensor misalignment and compensating.

In the PLL solution, a PLL is implemented with a single control loop to syncronize phases. The velocity is taken as a box average of the previously interpolated velocities which serves to migitage noise and discontinuity in estimation. Compared to the extrapolation method, here accuracy is traded off in return for smoothness. Since discontinuity results in rapid voltage and current spikes, the belief is that smoothness is preferable to accuracy. To maintain robust and reliable control, a fallback is implemented such that, when the PLL loses its lock (i.e. error from a hall transition is too large), the system falls back onto trapezoidal control until the PLL can regain a lock. This system behaves stably and reliably while also generating a smoother current waveform than the extrapolation method.

4.3 Hall Sensor Position Calibration

For both the extrapolation and PLL methods, hall sensor misalignment causes errors in rotor angle estimation. To mitigate the issue, the hall sensor alignments are calibrated by spinning the motor at a constant speed and recording the intervals between hall sensor transitions. It was found that not only were the hall sensors misaligned, but so were the permanent magnets in the rotor. This can be deduced by the observations that (a) the hall sensor timings change each rotation and (b) noticeable current spikes occur during FOC in a regular pattern of every 4 cycles corresponding to the fact that the motor is a 4 pole-pair motor. As a result, a calibration table consisting of 24 elements (4 sets of 6 transitions) was required. Figures 8 and 9 show the current waveforms for the extrapolation estimation method before and after calibrating hall sensor misalignment respectively.
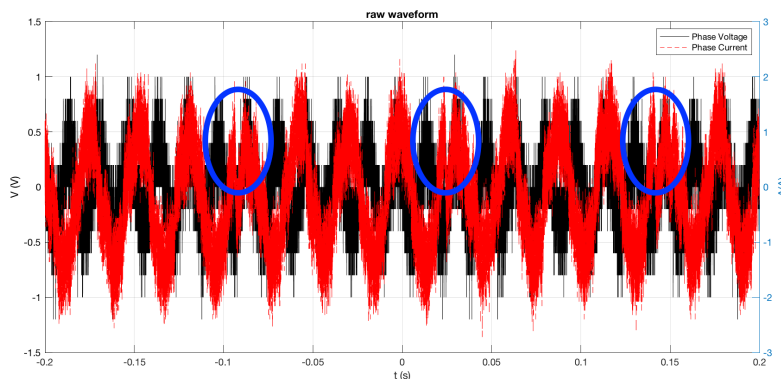

Figure 8: Periodic current anomolies occur every 4 cycles corresponding to the fact that the motor has 4 pole-pairs

4.4 Analysis of Techniques

When comparing the two methods of rotor angle estimation, we are primarily with two metrics: current RMS and noise. For each metric, we use trapezoidal control as a baseline in addition to the two estimation methods.
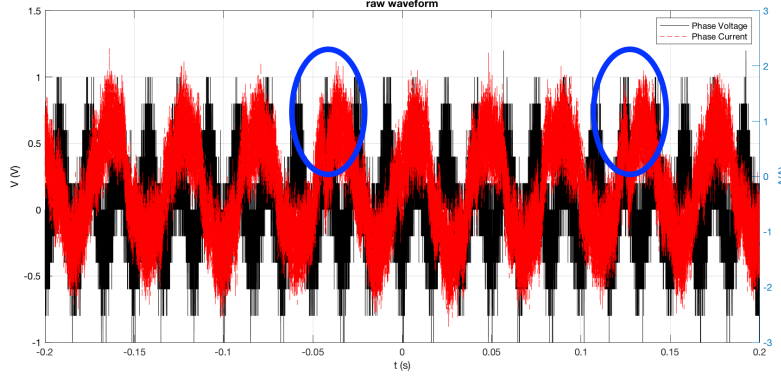
Figure 9: Periodic current anomolies are significantly reduced

Table 1: Rotor Angle Estimation Scheme Comparison

Control Scheme	Trapezoidal	FOC extrapolation	FOC PLL
Average Current (Arms)	2.170	1.587	1.495
Noise (Arms)	2.412	0.995	0.941

4.4.1 Quantitative Comparison

A more accurate rotor estimation scheme should result in a more efficient drive and therefore less average current consumption. The easiest way to measure this is to measure the RMS current required for each estimation scheme to spin the motor at a fixed speed and load. For convenience, a speed of 1760eRPM (80RPM @ 4 pole pairs and 5.5:1 gear ratio) and no-load condition was chosen.

A perfectly accurate rotor estimation scheme and FOC quadrature and direct current (Iq and Id, respectively) control loops would result in perfectly sinusoidal voltage and current waveforms. When small amounts of inaccuracy are introduced to the rotor angle estimation, large errors are observed in phase currents due to error in Park and inverse Park transformations and changing inductive properties from unexpected rotor positions. Therefore, phase current waveforms are expected to have significant deviation from a perfect sinusoid. Quantitatively, this noise can be measued as the output noise with 99.7% assurance after applying A-weighting [6].

The measurements for both average current consumption and noise are shown in Table 1. The average current measurements demonstrate that the FOC performs significantly more efficiently than the trapezoidal control and that, furthermore, the PLL estimation method outperforms the extrapolation method by 6.2%. The current noise measurements demonstrate that the FOC again outperforms trapezoidal by a large margin and that PLL again outperforms the extrapolation method, this time by 5.7%.

4.4.2 Qualitative Comparison

Figure 10 shows the estimated rotor positions using a first order extrapolation and using a PLL. Qualitatively, it is clear that the PLL generates a much smoother and qualitatively

11

better waveform. The quantitative results from Table 1 support this observation.

(a) Estimated rotor position using first order extrapolation
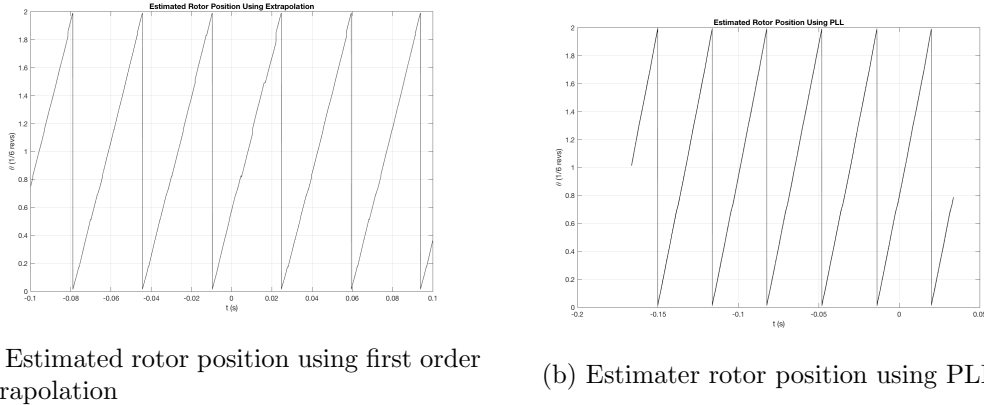

(b) Estimater rotor position using PLL

Figure 10: Comparison of estimated rotor positions using first order extrapolation and PLL

4.5   FOC PLL Fallback to Trapezoidal Control

In addition to the analyses of motor efficiencies using the aforementioned control schemes, the PLL control's fallback to trapezoidal control warrants additional discussion for its significant advantage of reliability. To ensure safe operation, it is necessary to smoothly transition to trapezoidal control when the PLL falls out of lock. Since a spinning motor must be powered by a matching bus voltage when running with trapezoidal control to minimize torque discontinuity, a system must be in place to correlate the existing throttle control from FOC to the required throttle control for trapezoidal control. This is problematic because FOC runs a control loop on quadrature current whereas trapezoidal control runs a control loop on bus voltage. Thus, a relationship between current and voltage must be established which facilitates a seamless handoff. Although a rigorous analysis should be done which takes into account current, voltage, torque, speed, and motor characteristics, a simple linear scaling between the two was found to suffice. Further analysis is to be completed and a more complex scheme may be implemented, but for the time being, the simplest possible scheme which maintains stable operation is preferable to maximize reliability. Figure 11 illustrates test cases where the PLL lost its lock for one hall transition and for multiple hall transitions. In each case, motor operation was uninterrupted and the speed was imperceptibly changed. It should be noted that an audible difference in operating noise was observed any time a switch occurred due to the trapezoidal control being significantly noisier and less efficient.

5   MMSPC for Motor Control Analysis

Earlier in this paper, MMSPC was purported to have significant advantages over traditional energy supply systems due to its ability to create finer granularity high power signals and self-balance. We will investigate the former advantage by making comparisons to a traditional DC bus system running with identical control schemes. This is made possible by switching each phase set consisting of four modules simultaneously effectively treating it as
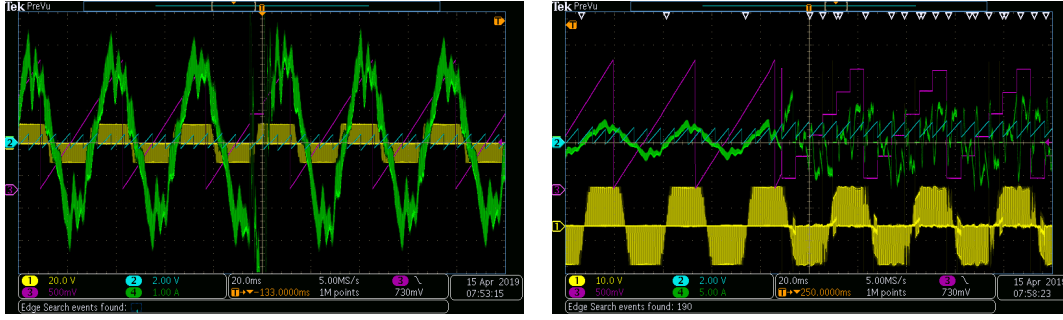
(a) FOC to trapezoidal handoff for a loss of lock in the PLL of one sector

(b) FOC to trapezoidal handoff for an extended loss of lock in the PLL

Figure 11: Fallback of FOC to trapezoidal control when PLL has lost its lock

Table 2: MMSPC Motor Control Comparison

Control	Trapezoidal		FOC extrapolation		FOC PLL	
Scheme	MMSPC	traditional	MMSPC	traditional	MMSPC	traditional
Average Current (Arms)	2.170	2.438	1.587	2.165	1.495	2.305
Noise (Arms)	2.412	2.964	0.995	2.086	0.941	2.086

a single module with the maximum voltage. Such a system is identical to the traditional 3 h-bridge, single DC bus BLDC motor control system.

Waveforms are provided in Figures 13, 14, and 15 comparing the MMSPC and traditional systems for trapezoidal, FOC extrapolated angle, and FOL PLL angle control schemes respectively. The results are summarized in Table 2. In every control scheme, we see that the MMSPC demonstrates clear advantages both in terms of power and noise. The best performance was achieved by the MMSPC running the FOC PLL control scheme which required only 61.3% of the current required by the most common commercial drive, the trapezoidal traditional system.

6 Conclusions

MMSPC systems have significant advantages in multiple domains. In this paper, we discussed the theoretical advantages of MMSPC systems in BLDC motor control applications. We then provided implementation details for a real-life system test and proceeded to show quantitatively that the MMSPC system's theoretical advantages are reflected in practice. Through the analysis, we have also begun the analysis of a promising new line of research in reliable motor control by fusing a fallback trapezoidal control and FOC by rotor angle estimation using hall sensors including hall sensor misalignment calibration.

Following these tests, a more rigorous analysis of the motor performance under load is to be conducted using an 0513-88802999 dynomometer. Upon successful completion of these tests, the system will be installed, on the test vehicle pictured in Figure 12 where it will undergo on-road tests for robustness, efficiency, and noise.

Figure 12: The long term goal of this project is to install the system on this vehicle.

References

[1] M. Cirrincione and M. Pucci. An mras-based sensorless high-performance induction motor drive with a predictive adaptive model. *IEEE Transactions on Industrial Electronics*, 52(2):532–551, April 2005.

[2] KA Corzine and SD Sudhoff. A hybrid observer for high performance brushless dc motor drives. *IEEE Transactions on Energy Conversion*, 11(2):318–323, 1996.

[3] S. M. Goetz, Z. Li, X. Liang, C. Zhang, S. M. Lukic, and A. V. Peterchev. Control of modular multilevel converter with parallel connectivity—application to battery systems. *IEEE Transactions on Power Electronics*, 32(11):8381–8392, Nov 2017.

[4] Shigeo Morimoto, Masayuki Sanada, and Yoji Takeda. Sinusoidal current drive system of permanent magnet synchronous motor with low resolution position sensor. In *IAS'96. Conference Record of the 1996 IEEE Industry Applications Conference Thirty-First IAS Annual Meeting*, volume 1, pages 9–14. IEEE, 1996.

[5] A. Tashakori and M. Ektesabi. A simple fault tolerant control system for hall effect sensors failure of bldc motor. In *2013 IEEE 8th Conference on Industrial Electronics and Applications (ICIEA)*, pages 1011–1016, June 2013.

[6] Hristo Zhivomirov. Noise measurement with matlab implementation, 2014.

A   Voltage and Current Waveforms for Various Control Schemes
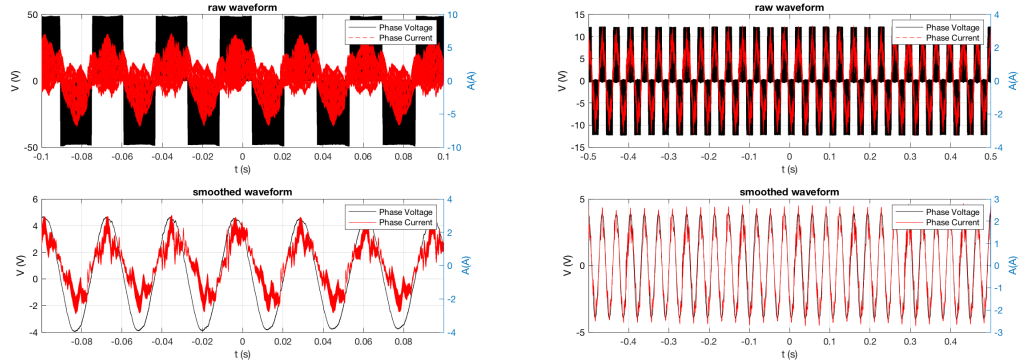
A.1   Trapezoidal Control
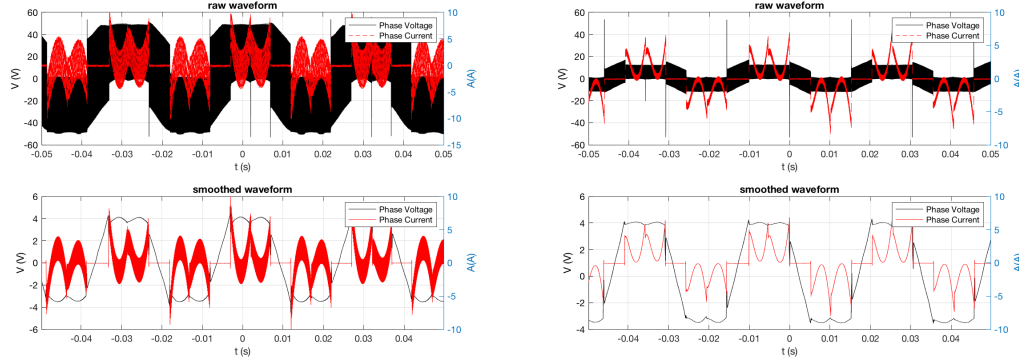
(a) Trapezoidal control without MMSPC

(b) Trapezoidal control with MMSPC

Figure 13: Comparison of trapezoidal control with and without MMSPC enabled

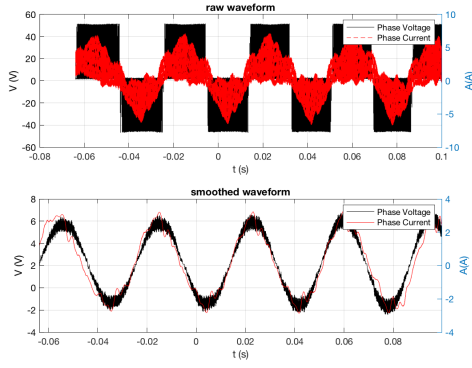## A.2   FOC First Order Extrapolation

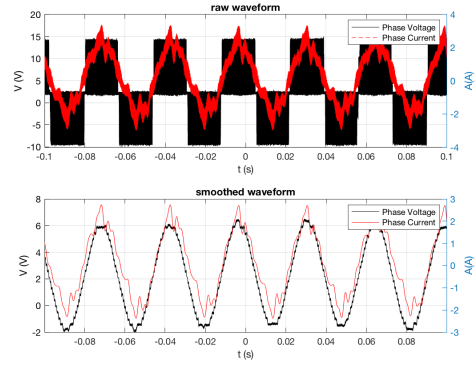(a) FOC using first order angle extrapolation without MMSPC

(b) FOC using first order angle extrapolation with MMSPC

Figure 14: Comparison of FOC control using first order extrapolation for angle estimation with and without MMSPC enabled

A.3   FOC PLL

(a) FOC using PLL for angle estimation without MMSPC

(b) FOC using PLL for angle estimation with MMSPC

Figure 15: Comparison of FOC control using PLL for angle estimation with and without MMSPC enabled